Original Article

Imaging Islets Labeled With Magnetic Nanoparticles at 1.5 Tesla

Joo Ho Tai,[1] Paula Foster,[2] Alma Rosales,[1] Biao Feng,[1] Craig Hasilo,[3] Violetta Martinez,[4] Soha Ramadan,[2] Jonatan Snir,[2] C.W. James Melling,[3] Savita Dhanvantari,[5] Brian Rutt,[2] and David J.G. White[1,3]

We have developed a magnetic resonance imaging (MRI) technique for imaging Feridex (superparamagnetic iron oxide [SPIO])-labeled islets of Langerhans using a standard clinical 1.5-Tesla (T) scanner and employing steady-state acquisition imaging sequence (3DFIESTA). Both porcine and rat islets were labeled with SPIO by a transfection technique using a combination of poly-L-lysine and electroporation. Electron microscopy demonstrated presence of SPIO particles within the individual islet cells, including β-cells and particles trapped between cell membranes. Our labeling method produced a transfection rate of 860 pg to 3.4 ng iron per islet, dependent on the size of the islet. The labeling procedure did not disrupt either the function or viability of the islets. In vitro 3DFIESTA magnetic resonance images of single-labeled islets corresponded with their optical images. In vivo T2*-weighted scan using 1.5 T detected as few as 200 SPIO-labeled islets transplanted under rat kidney capsule, which correlated with immunohistochemistry of the transplant for insulin and iron. Ex vivo 3DFIESTA images of kidneys containing 200, 800 or 2,000 SPIO-labeled islet isografts showed good correlation between signal loss and increasing numbers of islets. These data provide evidence that islets can be labeled with SPIO and imaged using clinically available 1.5-T MRI. *Diabetes* 55:2931–2938, 2006

From the [1]Department of Transplantation, Robarts Research Institute, London, Ontario, Canada; the [2]Imaging Research Laboratories, Robarts Research Institute, London, Ontario, Canada; the [3]Human Islet Transplantation Program, London Health Sciences Centre, London, Ontario, Canada; the [4]Department of Pathology, London Health Sciences Centre, London, Ontario, Canada; and the [5]Department of Medical Biophysics and Medicine, University of Western Ontario, Lawson Health Research Institute, London, Ontario, Canada.

Address correspondence and reprint requests to Dr. David J.G. White, FRCPath, PhD, Novartis/Stiller Professor of Xenotransplantation, Robarts Research Institute, Room 200, SDRI Building, University of Western Ontario, 1400 Western Rd., London, Ontario, Canada N6G 2V4. E-mail: david.white@robarts.ca.

Received for publication 23 March 2006 and accepted in revised form 25 July 2006.

J.H.T. and P.F. contributed equally to this work.

J.H.T. is currently affiliated with the Metabolism and Diabetes Imaging Program, Lawson Health Research Institute, St. Joseph's Hospital, London, Ontario, Canada.

HBSS, Hanks' balanced salt solution; ICP-MS, inductively coupled plasma mass spectrometry; ISG, insulin secretory granule; MRI, magnetic resonance imaging; PGFL, Phen Green FL; PLL, poly-L-lysine; SPIO, superparamagnetic iron oxide.

DOI: 10.2337/db06-0393

Successful β-cell replacement therapy, by pancreas or islet transplantation, is currently the only treatment that reestablishes endogenous insulin secretion responsive to normal feedback regulation, resulting in long-term normoglycemia (1,2). Pancreas transplantation alone for diabetes remains controversial due to the morbidity associated with the transplant (3). Significant progress has been made in human islet transplantation by the Edmonton group (4). However, many hurdles still remain that delay its widespread clinical use.

Potential causes of failure of islet transplants include failure of initial engraftment, inflammatory response at the transplant site, allo- or autoimmune response, and immunosuppressive drug-induced β-cell toxicity (1). In current clinical practice, isolated human islets from cadaveric donors are infused into the portal vein, which directly exposes them to the host bloodstream. This initiates an inflammatory reaction that activates both the complement and coagulation cascades causing islet damage and death (5,6). This may in part be due to the fact that isolated human islets do not express the complement regulatory protein, decay-accelerating factor (7). A number of alternate sites have been proposed as more suitable locations for islet transplantation. These include the spleen (8,9), the kidney capsule (9,10), the omental pouch (11), the gall bladder (12), intracerebrally (13), the rectum (14), mammary fat pads (15), and the testis (16). Locating the islets subcutaneously has also been advocated (17,18). Measures of success of the transplant other than the absolute measure of insulin independence would be helpful to assess function and outcomes (19). At present, assessment of graft function is dependent on clinical biochemistry, including measurement of C-peptide and glucose levels, intravenous glucose tolerance tests, intravenous arginine stimulation tests, and oral glucose tolerance tests (6). There is clearly a need for a noninvasive technique for quantifying islet graft survival in whatever location they may be transplanted in an accurate and reproducible manner.

High-resolution magnetic resonance imaging (MRI) can provide detailed anatomic information in a noninvasive way and is currently being used to characterize histopathology and morphologic phenotypes (20–23). MRI of superparamagnetic iron oxide (SPIO)-tagged cells has become a useful tool for studying cell trafficking in vivo (24–31). Areas containing SPIO-labeled cells appear as regions of low signal intensity on MRI images, creating

negative contrast. Heyn et al. (32,33) have recently shown that single SPIO-labeled cells can be detected in vivo. At present, there are few published reports of the use of MRI to image SPIO-labeled islets. Here, we describe a novel technique for SPIO labeling of islets and a unique system for cellular MRI at 1.5 Tesla (T), which utilizes a custom-built high-performance gradient coil insert and a 3D steady-state free precession imaging sequence. We demonstrate that individual SPIO-labeled islets can be easily visualized in vitro, and as few as 200 SPIO-labeled islets can be visualized after transplantation under the kidney capsule using a standard 1.5-T clinical MRI scanner.

RESEARCH DESIGN AND METHODS

Male Lewis rats were used as islet donors and recipients. Normal neonatal piglets were obtained from a farm in London, Ontario, Canada. All animals were housed in the University of Western Ontario animal facility in accordance with the guidelines established by the Canadian Council on Animal Care (34).

Isolation of islets. Rat islets were obtained from 6- to 8-week-old Lewis rats; porcine islets were isolated from 14- to 21-day-old piglets. The pancreas was removed by standard aseptic surgical techniques and chopped into 1- to 2-mm pieces (35–37). Tissue fragments were washed three times with Hanks' balanced salt solution (HBSS)/BSA and incubated for 10 min at 37°C with 1.0 mg/ml collagenase in HBSS/BSA. Tissue fragments were then washed twice in 30 ml HBSS/BSA at 4°C to remove collagenase and leaked exocrine-derived proteases. The tissue fragments were then incubated for 8 min at 37°C with 0.7 mg/ml collagenase in HBSS/BSA. The tissue fragments were then resuspended in 30 ml HBSS/BSA. Islets were separated from exocrine tissue by handpicking (35). Purity of the islet preparation is confirmed by dithizone staining of four random samples.

Islet labeling. Both rat and neonatal pig islets were labeled with the commercially available SPIO, Feridex (Berlex Laboratories). Feridex was complexed with poly-L-lysine (PLL; Sigma) to facilitate labeling (36). In addition, electroporation was tested as a method to enhance labeling efficiency. Briefly, Feridex (25 μg/ml) and PLL (1.5 μg/ml) were mixed with 1 ml culture medium using a rotator at 30 rpm for 1 h at room temperature. Neonatal porcine islets were gently mixed with labeling medium, transferred into a 0.4-cm Gene Pulser Cuvette (Bio-Rad Laboratories), and then electroporated at 100, 250, or 500 V with capacitance of 25 μF and infinite resistance (Gene Pulser Xcell; Bio-Rad). Electroporated samples were mixed with 5 ml complete culture medium in a 35 × 10-mm petri dish and incubated overnight at 37°C. For assessment of labeling efficiency, nine groups were compared: unlabeled islets; Feridex alone; Feridex plus PLL; Feridex plus electroporation with 100, 250, or 500 V; and Feridex plus PLL plus electroporation with 100, 250, or 500 V. Cell viability was measured in single-cell suspensions by trypan blue exclusion. All samples were counted in triplicate.

Quantification of cellular iron content by inductively coupled plasma mass spectrometry. Neonatal pig islets were dispersed into a single-cell suspension by trypsin and DNase I digestion. In eppendorf tubes, 5×10^5 single islet cells were resuspended in 2% gelatin. Iron content in single islet cells was determined using a Finnigan MAT Element High-Resolution inductively coupled plasma mass spectrometry (ICP-MS) system (Thermo Electron). Because of the large number of islets required (~18,000), these measurements could only be performed with pig islets since a neonatal pig pancreas will yield >30,000 islets. A typical rat pancreas yields ~400 islets (37).

Quantification of cellular iron content by fluorescence quenching. A novel flow cytometric quenching analysis was designed to measure intracellular iron content quickly and easily using the cell-permeant fluorescent indicator Phen Green FL (PGFL) (Invitrogen Molecular Probes). The intracellular fluorescence in cells labeled with PGFL is quenched by heavy metal ions in a concentration-dependent manner. Therefore, the presence of SPIOs results in the quenching of PGFL fluorescence. Briefly, 2×10^5 single SPIO-labeled islet cells were incubated with 1 μl PGFL for 20–30 min at 37°C and washed twice with PBS. After incubation, flow cytometry was performed to measure X-mean shift. This value was converted to relative percent of X-mean compared with control X-mean, then further calculated to the relative reduction (quenching) of fluorescence of PGFL as follows: relative quenching (%) = 100 − (flow cytometric X-mean of transfected islets/flow cytometric X-mean of control islets) × 100.

Histological and immunohistochemical staining and Prussian blue staining. Pancreas and kidneys were fixed in 10% formalin, embedded in paraffin, and 5-μm sections were prepared for histology. High-pressure heating with EDTA solution, pH 8.0, was used for antigen retrieval. Insulin was detected using a mouse anti-human antibody (NCL-Insulin; Novocastra Laboratories) at 1:50. Sections were incubated with the primary antibodies for 60 min at room temperature. After washing in PBS three times, the sections were incubated with mouse EnVision$^+$ polymer (DakoCytomation) for 30 min at room temperature. The sections were rinsed three times in PBS and were stained in diaminobenzidine solution (DakoCytomation) for 2–5 min at room temperature and counterstained with Mayer's hematoxylin (DakoCytomation). For Prussian blue staining, immunohistology sections were incubated with 2% potassium ferrocyanide in 6% HCl for 45 min.

Glucose stimulation index. The insulin secretory response to glucose was tested to determine the function of islets after labeling with SPIOs and electroporation. Briefly, after an overnight culture in RPMI-1640, 20 islets were handpicked. The islets were transferred into a 15-ml tube and incubated in 1.5 ml RPMI-1640 containing 2.8 mmol/l glucose for 60 min at 37°C. The samples were centrifuged for 4 min at 100 rpm and the supernatant was removed for measurement of insulin concentration by enzyme-linked immunosorbent assay (ALPCO Diagnostics). The islets were resuspended in RPMI-1640 containing 20 mmol/l glucose and the procedure repeated. The stimulation index was defined as a ratio of insulin release stimulated by 20 mmol/l glucose to 2.8 mmol/l glucose. All experiments were performed in triplicate.

Electron microscopy. Labeled and unlabeled neonatal pig islets were handpicked under a stereoscope (SMZ-2B; Nikon) and fixed in 2.5% glutaraldehyde in PBS and postfixed in 1% OsO_4. For microscopy of SPIO particles alone, a Feridex suspension was mixed in culture medium for 1 h, fixed as above, and spun down at 130,000 rpm for 1 min. Ultra-thin sections were stained with uranyl acetate and lead citrate and examined with a Philips 410 electron microscope.

Samples for in vitro MRI and optical imaging. To facilitate correlative in vitro MRI and optical imaging, 1–10 SPIO-labeled neonatal porcine islets/islet clusters were handpicked and placed in a single plane sandwiched between a bottom layer of 8% (wt/wt) gelatin and a top layer of 2% gelatin in a 350-μl optically transparent plastic microwell. All islet/islet clusters were again confirmed by dithizone staining after handpicking and before loading the phantoms. Optical images for each well were obtained using a stereoscope (SMZ-2B; Nikon) with low magnification.

Renal subcapsular transplantation of islets in Lewis rats. Feridex-labeled islets isolated from Lewis rats were isografted beneath the renal capsule of the left kidney of recipient Lewis rats using a previously described protocol (38). Three different numbers of labeled islets were transplanted: 200, 800, and 2,000. The right kidney was used as a control.

MRI. All imaging was performed on a 1.5-T General Electric EXCITE system. Rats were anesthetized with ketamine/xylazine (0.1 ml per 100 g body wt) and positioned on a 3-in surface radiofrequency coil. Multislice 2D T2*-weighted gradient echo images were acquired with repetition time/echo time (TR/TE) = 250/25 ms, 512 × 256 matrix, four averages, and 0.5-mm slice thickness. Images were acquired once per week for up to 5 weeks. After the last imaging session, kidneys were removed and fixed in 10% formalin for ex vivo imaging. Imaging of gel samples and ex vivo kidney specimens was performed using a custom-built, high-performance gradient coil insert (inner diameter 12 cm, maximum gradient strength 600 mT/m, and peak slew rate 2,000 $T \cdot m^{-1} \cdot s^{-1}$). Solenoidal radiofrequency coils were custom built to hold the well sample and the ex vivo kidney sample with dimensions just larger than the regions to be imaged. These samples were scanned with the 3DFIESTA pulse sequence with the following parameters: TR/TE = 7.8/3.9 ms, flip angle 50°, 21-kHz bandwidth, 4–24 signal averages, and spatial resolution of 100 × 100 × 200 μm. The average contrast from regions of signal void was measured using an image analysis package (ImageJ; National Institutes of Health). Signal void contrast was expressed as the percent signal drop compared with background tissue and was calculated by taking the signal difference between background tissue and the signal void, dividing by the background signal, and multiplying this fractional signal loss by 100.

Statistical analysis. Data were analyzed with an unpaired *t* test with Welch's correction, ANOVA, and Spearman's correlation coefficients, where appropriate.

RESULTS

Islet labeling. Table 1 shows iron concentrations in islets as determined by ICP-MS after islet labeling and cell viability after each labeling procedure. Statistical analysis of the ICP-MS iron concentration data showed that all sample groups, including the control group, were significantly different from each other ($P < 0.01$), except for the pair of Feridex only and Feridex plus 100 V. These data show a clear advantage for the use of PLL over electropo-

TABLE 1
Relative efficiency of different methods of Feridex labeling of porcine islets

Group	ICP-MS for iron		
	Concentration (pg/cell)	Relative increase*	Islet cell viability (%)†
n	8		3
Control	0.091 ± 0.002	1.00	94.7 ± 1.3[a,b]
Feridex only	0.126 ± 0.003[c]	1.38	94.3 ± 3.9[d,e]
Feridex plus PLL	1.005 ± 0.021	11.04	97.0 ± 1.1[f,g]
Feridex plus 100 V	0.123 ± 0.003[c]	1.35	94.9 ± 2.2[h,i]
Feridex plus 250 V	0.262 ± 0.006	2.88	85.6 ± 4.2[a,d,f,h,j]
Feridex plus 500 V	0.210 ± 0.004	2.31	81.1 ± 2.8[b,e,g,i,k,l,m]
Feridex plus PLL plus 100 V	0.630 ± 0.013	6.92	90.5 ± 2.5[k]
Feridex plus PLL plus 250 V	1.269 ± 0.027	13.96	94.7 ± 2.9[j,l]
Feridex plus PLL plus 500 V	1.724 ± 0.036	18.96	91.4 ± 0.9[m]

Data are means ± SD. *The relative increases were calculated by mean iron concentration of each sample group/mean iron concentration of the control group. †Viability was examined before gel sample preparation for ICP-MS. [a, d, h, j, k] $P < 0.05$ vs. another corresponding group. [b, c, e, f, g, i, l, m] $P < 0.01$ vs. another corresponding group.

ration alone. This increase in the labeling efficiency of PLL was further enhanced by electroporation at voltages of 250 or 500 V. Analysis of the viability data (Table 1) showed that electroporation at 250 and 500 V significantly decreased cell viability compared with controls. However, the addition of PLL significantly ($P < 0.01$) enhanced the viability of islets subjected to electroporation at 250 and 500 V. These results suggest that PLL might play a role in protecting islets from the electric shock when used with electroporation. The highest iron labeling as measured by ICP-MS was achieved in the Feridex plus PLL plus 500 V group as 1.72 pg of SPIO per single islet cell based on the total number of cells measured (5×10^5) and the total amount of iron detected. On the basis that an islet can contain between 500 and 2,000 cells, our labeling technique will load a single islet with between 870 pg and 3.48 ng SPIO, which is well in excess of the amount needed for detection by MRI. We also developed a rapid and simple measurement to confirm successful intracellular islet labeling. This technique uses the quenching properties of iron on the fluorescence of PGFL. PGFL fluoresces only upon cleavage of its diacetate moieties by intracellular esterases. Therefore, PGFL fluorescence will be quenched only by iron within the cell and not particles adhering to the cell membrane. Since our studies have shown that SPIOs can adhere to the cell membrane (infra vide), this quenching methodology cannot be compared directly with the determination of iron content by ICP-MS. Surprisingly, the two methodologies show a significant correlation (Spearman's rho = 0.72, $P < 0.05$) (Fig. 1). Although this correlation is not strong, this technique does provide a rapid method for determining the success of a labeling procedure.

Stimulation index as functional studies. Glucose-stimulated insulin release in SPIO-labeled (Feridex plus PLL plus 250 V) and nonlabeled islets are shown in Fig. 2*A* for rat islets and Fig. 2*B* for neonatal pig islets. There was no difference in stimulation indexes between the Feridex-labeled rat islet group (1.51 ± 0.54) and the nonlabeled islet group (1.20 ± 0.13) or between the Feridex-labeled neonatal pig islet group (2.87 ± 0.06) and the nonlabeled control group (1.72 ± 0.19), indicating labeling of islets with SPIOs using our combination methods does not affect glucose-stimulated insulin secretion.

Electron microscopy. We examined the morphology of SPIO particles using electron microscopy (Fig. 3*A*). The characteristic granular morphology of these SPIO particles was identified only in SPIO-labeled islets and never in unlabeled controls (data not shown). Figure 3 shows that the unique appearance of SPIO particles is quite distinct

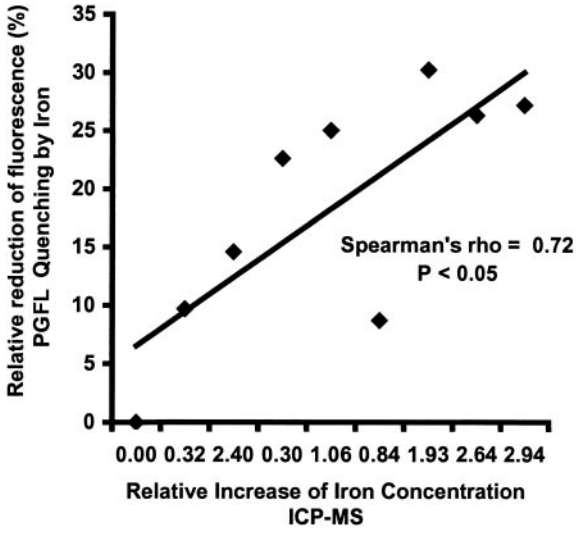

FIG. 1. Correlation between relative Phen Green FL (PGFL) quenching by iron using flow cytometry and relative increase of iron concentration from ICP-MS in SPIO-labeled neonatal pig single islet cells.

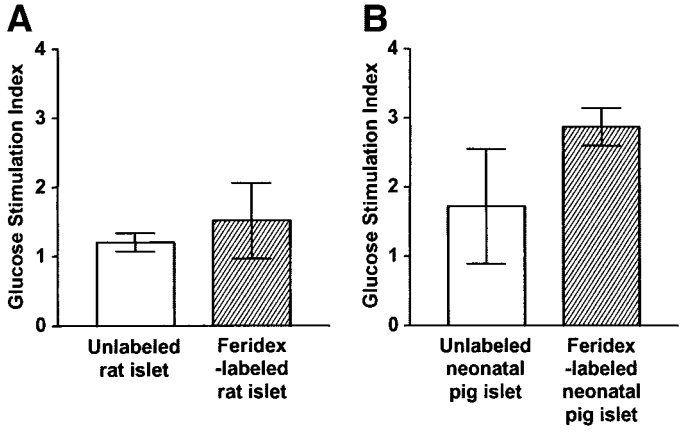

FIG. 2. Glucose stimulation index of SPIO-labeled and unlabeled rat (*A*) and neonatal porcine (*B*) islets ($n = 3$).

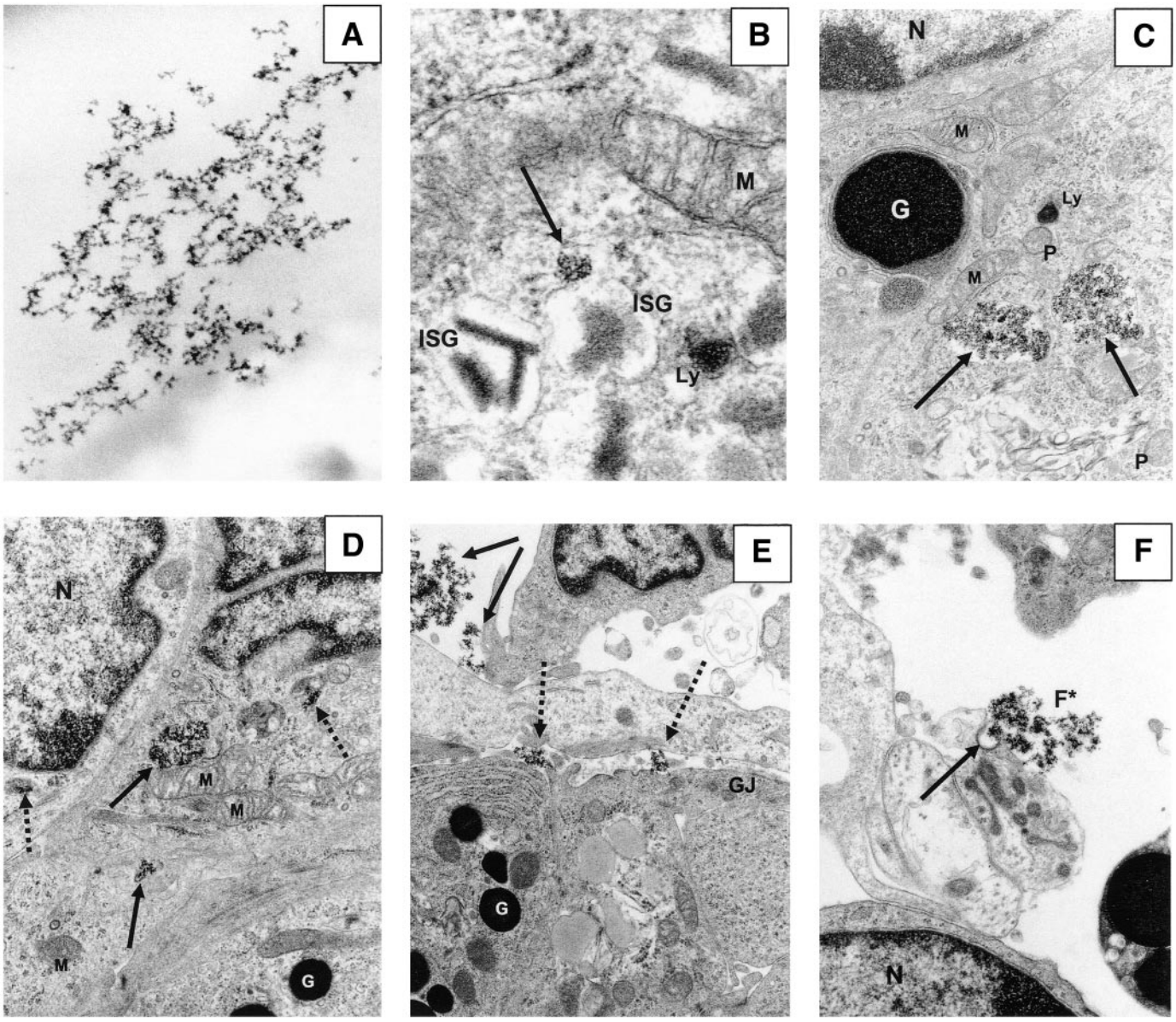

FIG. 3. Electron microscopy of neonatal pig islets labeled with Feridex using PLL and electroporation (500 V). *A*: Feridex particles alone are electron dense and display a unique granular morphology, ×84,861. *B*: Feridex particles in an endosome (arrow) detected in the cytoplasm of β-cells and located above an ISG. Ly, lysosome; M, mitochondria containing cristae; ×82,410. *C*: Feridex particles (arrows) in the cytoplasmic endosome of δ-cells. G, dense granule; N, nucleus; P, normal peroxisome; ×41,205. *D*: Feridex particles in the cytoplasmic endosomes in δ-cells (arrows) and peroxisome-like organelles (dotted arrows); ×41,205. *E*: Feridex particles trapped between α-cells and other islet cells (dotted arrows) located in the periphery of islets and associated with gap junctions (GJ; arrows) between two cells; ×35,178. *F*: Feridex particles (F*) undergoing endocytosis (arrow); ×41,205.

from the morphology of other organelles, such as the nucleus, mitochondria, lysosomes, and insulin secretory granules (ISGs). ISGs in porcine β-cells contain a characteristic electron-dense bar-shaped crystal (Fig. 3*B*). SPIO particles were observed in the cytoplasm of β-cells (located in the center of the islet, Fig. 3*B*), δ-cells (Fig. 3*C*), on α-cells (Fig. 3*E*), and in nongranular cells (Fig. 3*D*) that could be either chromophobic C-cells or acinar cells. The subcellular distribution of SPIO particles was mainly throughout the cytoplasm and lysosomes of islet cells. The number of SPIO-labeled cells was decreased deep within the islet cell mass. Of particular interest was the observation that SPIO particles were attached to the cell membrane or trapped between cells (Fig. 3*E*). Figure 3*F* shows endocytosis of SPIO particles.

MRI. Individual SPIO-labeled islets/islet clusters were easily visualized in 3DFIESTA images of gel samples (Fig. 4*A–C*). A comparison of the optical images of the gel samples showed good correspondence with the magnetic resonance images (Fig. 4*D–F*). The fractional signal loss measured for the islets/islet clusters labeled 1–7 are 69.7, 62.1, 55.6, 47.2, 51.5, 62.7, and 79%, respectively. In Fig. 5, representative in vivo T2*-weighted General Electric images are shown for rats transplanted with 2,000 and 200 islets. A small focal region of signal loss is apparent at the site of the transplant of 200 islets (Fig. 5*B*, arrow). The fractional signal loss measured for this region was 64.4% at week 1 and 68.8% at week 5. No qualitative changes in the appearance of this region of signal loss were apparent over the course of the 5 weeks (data not shown). The region of

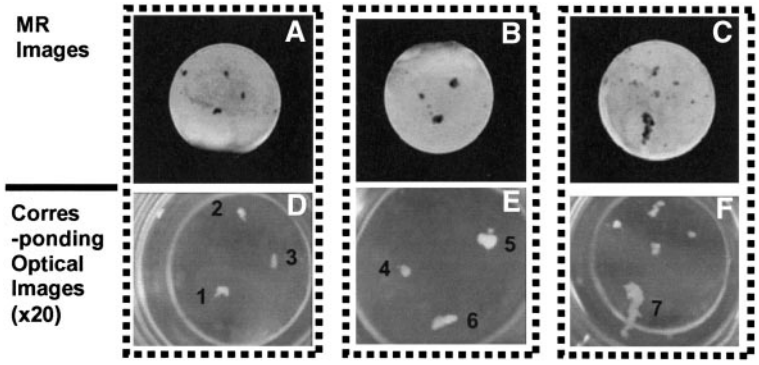

FIG. 4. 3DFIESTA magnetic resonance (MR) images (*A–C*) of isolated, SPIO-labeled neonatal pig islets placed in 2% phantom gelatin of plastic wells. Corresponding optical images (*D–F*, ×20) were matched with MRI images (*A–C*). The islets/islet clusters numbered 1–7 (*D–F*) were analyzed for the fractional signal loss.

signal loss caused by the transplantation of 2,000 islets is much larger and much more obvious (Fig. 5*A*). All of the different numbers of transplanted islets could be visualized in ex vivo 3DFIESTA images of kidneys (Fig. 6). As expected, the greater the number of islets in the transplant, the larger the region of signal loss appeared. The 200-islet transplant was the only case where it appeared that individual islet clusters could be detected from both the sagittal and coronal views of the kidney (Fig. 6*A* and *B*). In the coronal view (Fig. 6*B*), a line of islets is apparent at the transplant site. The sagittal view of kidney with 800 SPIO-labeled islets transplanted (Fig. 6*C*) shows a large region of signal loss, completely obliterating signal from the kidney capsule. In Fig. 6*D* and *E*, the same effect is shown in the 2,000-islet transplant. Characteristic magnetic field lines resulting form the large concentration of iron are apparent. The 3DFIESTA images of fixed kidneys with 200, 800, and 2,000 transplanted islets are shown after 3D rendering (Fig. 7). The islets are shown in red. In the image of the kidney with 200 islets, the islet cell clusters can be easily visualized and counted (Fig. 7*A*). A total of 35 discrete regions were counted. The fractional signal loss was measured for each of these regions. The mean fractional signal loss was 73.8%. In 3DFIESTA images of the 800 and 2,000 islet transplants, discrete regions of signal loss were not observed because of the blooming artifact

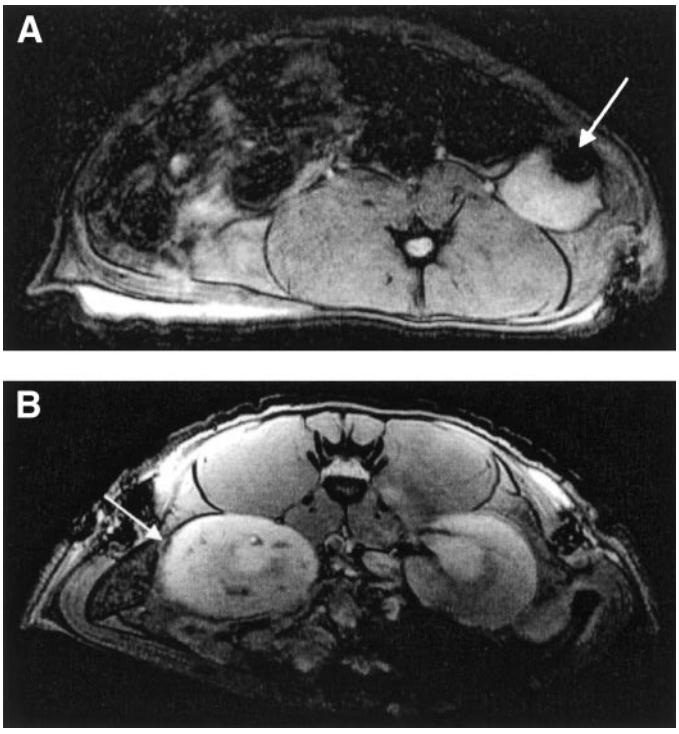

FIG. 5. In vivo T2*-weighted gradient echo image. *A*: Lewis rat transplanted with SPIO-labeled 2,000 islet isografts under kidney capsules. The very high iron concentration in this region leads to a large blooming artifact in these gradient echo images (arrow). *B*: Lewis rat transplanted with 200 SPIO-labeled islet isografts in the kidney subcapsular area, showing the black signal void of SPIO-labeled islets surrounded by the capsule (arrow).

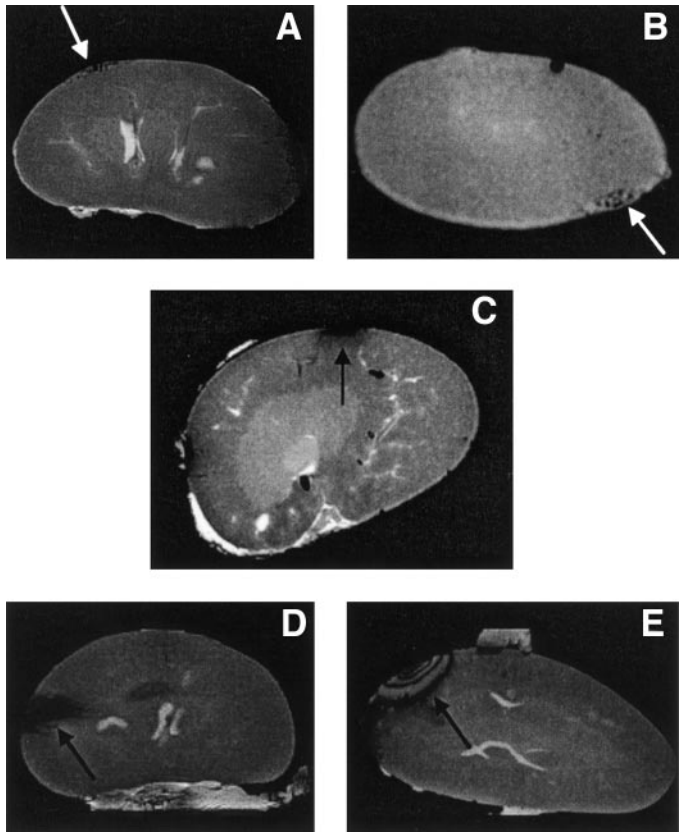

FIG. 6. Ex vivo 3DFIESTA magnetic resonance image of Lewis rat kidney transplanted with Feridex-labeled islet isografts into the renal subcapsular area (arrows). *A* and *B*: A sagittal and a coronal scan, respectively, for 200 SPIO-labeled islets. *C*: A sagittal scan for 800 SPIO-labeled islets. *D* and *E*: A sagittal and a coronal scan, respectively, for 2,000 SPIO-labeled islets, showing characteristic iron artifacts (*E*).

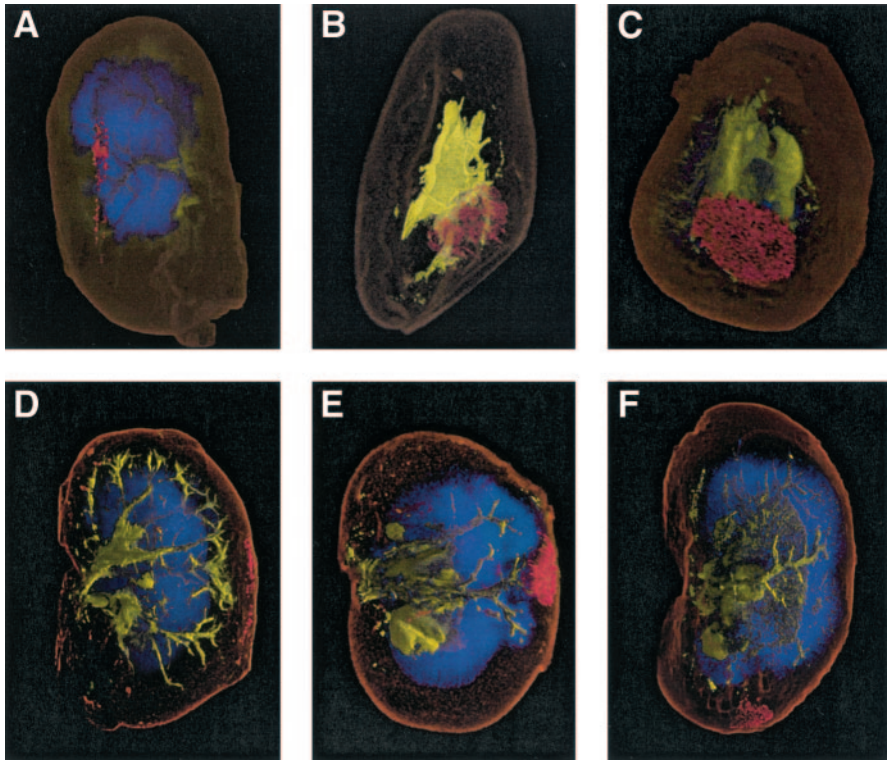

FIG. 7. The ex vivo 3D color FIESTA magnetic resonance images of 200 (*A* and *D*), 800 (*B* and *E*), and 2,000 (*C* and *F*) SPIO-labeled islet isografts in the Lewis rat kidney capsule. *A–C*: Individual frames selected from 3D animation of the magnetic resonance data to show maximum signal loss. *D–F*: Individual frames selected to illustrate the transplanted region under the kidney capsule. The islets are shown in red. The medulla appears blue; the major and minor calyx together with the renal vein, artery, and their associated smaller vessels appear yellow.

(Fig. 7*B* and *C*). Signal intensity was therefore measured from the whole region of signal loss. The average fractional signal loss was 83.2% for the 800-islet transplant and 88% for the 2,000-islet transplant.

Histology and immunohistochemistry. The location of SPIO-labeled islets in the renal subcapsular area was confirmed by immunohistochemistry for insulin and Prussian blue staining (Fig. 8). The presence of insulin immunoreactivity in islet isografts was detected at day 36 posttransplantation (Fig. 8*A*). The colocalization staining of iron detected by Prussian blue with anti-insulin antibody revealed SPIO within β-cells, as well as outside β-cells (Fig. 8*B*).

DISCUSSION

In this article, we show that MRI can be used to visualize individual SPIO-labeled islets/islet clusters in vitro in gel and small numbers of SPIO-labeled islets after their transplantation under the kidney capsule. The magnetic susceptibility of SPIO particles produces magnetic field inhomogeneities that are known to affect regions in magnetic resonance images over a far greater area than the actual particle distribution. Large collections of SPIO-labeled cells can influence magnetic resonance signal intensity many pixels away and produce an effect described as blooming artifact. The size of the blooming artifact is pulse-sequence and field-strength dependent. To maximize the ability to visualize this effect, most imaging studies have used T2- or T2*-weighted spin echo and gradient echo pulse sequences and high magnetic field strengths. The region of signal void in these magnetic resonance images is consequentially larger than the actual area occupied by the iron labeled cells.

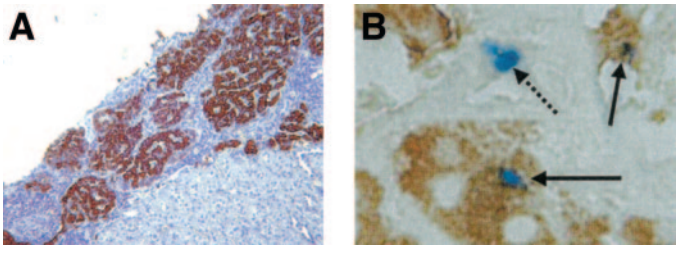

FIG. 8. Immunohistochemistry for insulin (brown) in a Lewis rat kidney isografted with 200 SPIO-labeled islets beneath the kidney capsule (*A*; ×50). Colocalization of Prussian blue staining for iron (blue) and insulin immunoreactivity (brown) in the isograft revealed the presence of SPIO iron particles in the insulin-producing β islet cells (arrows, blue in brown) and in other regions of the transplant (dotted arrow, blue) at day 36 after SPIO-labeled islet transplantation (*B*; ×400).

Our in vivo images of the rat kidneys were acquired with a T2*-weighted gradient echo pulse sequence. A decrease in signal intensity was observed at the site of transplantation, which was observed for at least 5 weeks following the transplantation. However, our images of the ex vivo kidneys and of isolated islets in gel were acquired with a specialized, custom-built gradient coil insert and a 3DFIESTA imaging sequence. The 3DFIESTA imaging sequence has a number of advantageous features, over other imaging sequences, for certain cellular imaging applications. What was originally considered a negative aspect of this imaging sequence, the high sensitivity to off-resonance effects, has made it very effective for cellular imaging with iron oxide nanoparticles. Recently, we demonstrated for the first time that individual SPIO-labeled cells can be detected in vivo using this specialized microimaging approach (32). This sequence exhibits blooming artifact suppression traits intrinsic to spin echo sequences, while

maintaining the sensitivity to iron oxide–labeled cells intrinsic to gradient echo sequences.

In addition, the 3DFIESTA sequence provides substantially enhanced signal-to-noise ratio, relative to spin echo and gradient echo sequences. This improvement in signal-to-noise ratio allows for microimaging at lower field strengths than is typically possible and for the acquisition of images at high spatial resolution with reasonable scan times. These two factors were key to our ability to visualize small numbers of iron-labeled cells in islets in vitro and ex vivo.

Our electron microscope analysis revealed that all major types of islet cells contained Feridex particles. Since many of the organelles and granules in islet cells possess a similar electron density and appearance as iron oxide nanoparticles, we looked at the electron microscope of Feridex alone to allow accurate identification of the presence of Feridex in islet cells. We have shown localization of SPIO in the cytoplasm of islet cells, including β-cells under electron microscope. This finding is consistent with the reported colocalization of SPIO-associated fluorescence with endosomal markers or Cy5.5 signal from MN-NIRF (magnetic nanoparticles modified with the near-infrared fluorescent Cy5.5 dye) probe and insulin in grafted human islets (39). Our electron microscope study also showed that Feridex nanoparticles can be observed between islet cells and beside gap junctions. It is important to point out that the electron density and appearance of the immature ISGs in β-cells resembles those of Feridex. The similarity in appearance of iron-labeled islet cells and normal (immature or developing) ISGs has led to some confusion regarding subcellular location of SPIO in the cytoplasm. One study (40) claimed that SPIO particles were present in lysosomes in β-cells of isolated rat islets. However, this claim was subsequently retracted as it appears that their technique was limited to labeling macrophages within the islet (41). Our electron microscope analysis has now clarified the location of SPIO within islet cells.

Our analysis of Feridex transfection efficiency using ICP-MS and PGFL quenching demonstrated that combining PLL with electroporation increased the iron load incorporated into the islet while maintaining viability. The highest labeling efficiency was found when PLL was used with electroporation at 500 V. We determined the iron content in 5×10^5 single islet cells to be an average of 1.72 pg per cell. This average, however, disguises the fact that our electron microscope study shows some cells to be unlabeled, while others, notably those on the periphery of the islet, to be heavily labeled. However, based on this average, the total iron content for an islet that may vary in size from 500 to 2,000 cells would be between 860 pg and 3.4 ng, which is well in excess of the amount needed for in vivo imaging. Our electron microscope analysis also showed that Feridex particles were observed trapped between islet cells. These particles are likely lost during the single islet cell preparation for iron content analysis, and, as a result, the actual amount of Feridex in the labeled islets is expected to be slightly higher than that measured in the single cells by ICP-MS and could account for the modest correlation between PGFL quenching and ICP-MS measurements. PGFL quenching, however, does provide a rapid and simple check for the successful SPIO labeling of an islet population.

Jirak et al. (40) claimed that rat islets could be labeled with SPIO without transfection by incubation of 140 μg/ml for 2 days. They reported a final cell labeling of 90 pg Feridex per cell. Our results are more consistent with the results of a recent study by Moore et al. (39) in which a range of 2–12 pg Feridex per cell was achieved for human islets labeled by an overnight incubation with 10–300 μg/ml of a novel SPIO agent carrying the optical dye Cy5.5. In our study, we have consistently used 25 μg/ml SPIO. This has not led to any toxicity since the stimulation index for rat islets showed no difference between Feridex-labeled islets and unlabeled islets with a viability of 92%. Therefore, using 10 times less SPIO for labeling, our results are in agreement with the results by Moore et al. (39), and our transfection method using PLL and electroporation made it possible to deliver SPIO into all islet cell cytoplasm (transfection) and labeling (attachment on the cell membrane). In addition, the histology of the islets 36 days posttransplant shows staining for insulin. We have also shown colocalization of iron staining and insulin in islets after transplantation.

Using the technique described here, it should be possible to Feridex label a small number of islets, which can then be mixed in with cells used in an islet transplant and subsequently imaged to stand as a surrogate for the overall fate of the transplant. The concept of labeling a proportion of the islets is a strategy for minimizing the blooming artifact associated with a large islet graft observed in our 3DFIESTA images.

ACKNOWLEDGMENTS

This work was funded by grants from the Alan Thicke Foundation, Ontario Research Development Challenge Fund, and the Canadian Diabetes Association.

We thank Tracy Hill and other members in the Animal Care and Veterinary Service at the University of Western Ontario for assistance in animal surgery, Hongtao Sun for immunohistochemistry, Colin Bradley for ICP-MS measurements, and Yunkyung Cho for help with statistical analysis.

REFERENCES

1. Robertson RP, Davis C, Larsen J, Stratta R, Sutherland DE: Pancreas and islet transplantation for patients with diabetes. *Diabetes Care* 23:112–116, 2000
2. Lakey JR, Burridge PW, Shapiro AM: Technical aspects of islet preparation and transplantation. *Transpl Int* 16:613–632, 2003
3. Venstrom JM, McBride MA, Rother KI, Hirshberg B, Orchard TJ, Harlan DM: Survival after pancreas transplantation in patients with diabetes and preserved kidney function. *JAMA* 290:2817–2823, 2003
4. Shapiro AM, Lakey JR, Ryan EA, Korbutt GS, Toth E, Warnock GL, Kneteman NM, Rajotte RV: Islet transplantation in seven patients with type 1 diabetes mellitus using a glucocorticoid-free immunosuppressive regimen. *N Engl J Med* 343:230–238, 2000
5. Bennet W, Sundberg B, Groth CG, Brendel MD, Brandhorst D, Brandhorst H, Bretzel RG, Elgue G, Larsson R, Nilsson B, Korsgren O: Incompatibility between human blood and isolated islets of Langerhans: a finding with implications for clinical intraportal islet transplantation? *Diabetes* 48: 1907–1914, 1999
6. Bennet W, Sundberg B, Lundgren T, Tibell A, Groth C, Richards A, White D, Elgue G, Larsson R, Nilsson B, Korsgren O: Damage to porcine islets of Langerhans after exposure to human blood in vitro, or after intraportal transplantation to cynomologous monkeys: protective effects of sCR1 and heparin. *Transplantation* 69:711–719, 2000
7. Bennet W, Bjorkland A, Sundberg B, Brandhorst D, Brendel MD, Richards A, White DJ, Nilsson B, Groth CG, Korsgren O: Expression of complement regulatory proteins on islets of Langerhans: a comparison between human islets and islets isolated from normal and hDAF transgenic pigs. *Transplantation* 72:312–319., 2001
8. Scharp DW, Marchetti P, Swanson C, Newton M, McCullough CS, Olack B: The effect of transplantation site and islet mass on long-term survival and

metabolic and hormonal function of canine purified islet autografts. *Cell Transplant* 1:245–254, 1992
9. Bretzel RG, Flesch BK, Brennenstuhl G, Greiner I, Hering BJ, Woehrle M, Federlin K: Rat pancreatic islet pretreatment with anti-MHC class II monoclonal antibodies and culture: in vitro MLIC test response does not predict islet allograft survival. *Acta Diabetol* 30:49–56, 1993
10. Mellgren A, Schnell Landstrom AH, Petersson B, Andersson A: The renal subcapsular site offers better growth conditions for transplanted mouse pancreatic islet cells than the liver or spleen. *Diabetologia* 29:670–672, 1986
11. Kin T, Korbutt GS, Rajotte RV: Survival and metabolic function of syngeneic rat islet grafts transplanted in the omental pouch. *Am J Transplant* 3:281–285, 2003
12. Simeonovic CJ, Dhall DP, Wilson JD, Lafferty KJ: A comparative study of transplant sites for endocrine tissue transplantation in the pig. *Aust J Exp Biol Med Sci* 64:37–41, 1986
13. Tze WJ, Tai J: Intracerebral allotransplantation of purified pancreatic endocrine cells and pancreatic islets in diabetic rats. *Transplantation* 38:107–111, 1984
14. Lim SM, Li SQ, Poh LH, Lim NK, Seah ML, Heng KK: The rectum as a novel site for islet cell transplantation. *Transplantation* 57:294–296, 1994
15. Outzen HC, Leiter EH: Transplantation of pancreatic islets into cleared mammary fat pads. *Transplantation* 32:101–105, 1981
16. Ferguson J, Scothorne RJ: Extended survival of pancreatic islet allografts in the testis of guinea-pigs. *J Anat* 124:1–8, 1977
17. Kawakami Y, Iwata H, Gu Y, Miyamoto M, Murakami Y, Yamasaki T, Cui W, Ikada Y, Imamura M, Inoue K: Modified subcutaneous tissue with neovascularization is useful as the site for pancreatic islet transplantation. *Cell Transplant* 9:729–732, 2000
18. Wang W, Gu Y, Hori H, Sakurai T, Hiura A, Sumi S, Tabata Y, Inoue K: Subcutaneous transplantation of macroencapsulated porcine pancreatic endocrine cells normalizes hyperglycemia in diabetic mice. *Transplantation* 76:290–296, 2003
19. Ryan EA, Lakey JR, Paty BW, Imes S, Korbutt GS, Kneteman NM, Bigam D, Rajotte RV, Shapiro AM: Successful islet transplantation: continued insulin reserve provides long-term glycemic control. *Diabetes* 51:2148–2157, 2002
20. Johnson GA, Benveniste H, Black RD, Hedlund LW, Maronpot RR, Smith BR: Histology by magnetic resonance microscopy. *Magn Reson Q* 9:1–30, 1993
21. Johnson GA, Cofer GP, Fubara B, Gewalt SL, Hedlund LW, Maronpot RR: Magnetic resonance histology for morphologic phenotyping. *J Magn Reson Imaging* 16:423–429, 2002
22. Gareau PJ, Wymore AC, Cofer GP, Johnson GA: Imaging inflammation: direct visualization of perivascular cuffing in EAE by magnetic resonance microscopy. *J Magn Reson Imaging* 16:28–36, 2002
23. Johnson GA, Cofer GP, Gewalt SL, Hedlund LW: Morphologic phenotyping with MR microscopy: the visible mouse. *Radiology* 222:789–793, 2002
24. Moore A, Josephson L, Bhorade RM, Basilion JP, Weissleder R: Human transferrin receptor gene as a marker gene for MR imaging. *Radiology* 221:244–250, 2001
25. Moore A, Sun PZ, Cory D, Hogemann D, Weissleder R, Lipes MA: MRI of insulitis in autoimmune diabetes. *Magn Reson Med* 47:751–758, 2002
26. Moore A, Marecos E, Bogdanov A Jr, Weissleder R: Tumoral distribution of long-circulating dextran-coated iron oxide nanoparticles in a rodent model. *Radiology* 214:568–574, 2000
27. Lewin M, Carlesso N, Tung CH, Tang XW, Cory D, Scadden DT, Weissleder R: Tat peptide-derivatized magnetic nanoparticles allow in vivo tracking and recovery of progenitor cells. *Nat Biotechnol* 18:410–414, 2000
28. Bulte JW, Zhang S, van Gelderen P, Herynek V, Jordan EK, Duncan ID, Frank JA: Neurotransplantation of magnetically labeled oligodendrocyte progenitors: magnetic resonance tracking of cell migration and myelination. *Proc Natl Acad Sci U S A* 96:15256–15261, 1999
29. Dodd CH, Hsu HC, Chu WJ, Yang P, Zhang HG, Mountz JD Jr, Zinn K, Forder J, Josephson L, Weissleder R, Mountz JM, Mountz JD: Normal T-cell response and in vivo magnetic resonance imaging of T cells loaded with HIV transactivator-peptide-derived superparamagnetic nanoparticles. *J Immunol Methods* 256:89–105, 2001
30. Dousset V, Delalande C, Ballarino L, Quesson B, Seilhan D, Coussemacq M, Thiaudiere E, Brochet B, Canioni P, Caille JM: In vivo macrophage activity imaging in the central nervous system detected by magnetic resonance. *Magn Reson Med* 41:329–333, 1999
31. Dodd SJ, Williams M, Suhan JP, Williams DS, Koretsky AP, Ho C: Detection of single mammalian cells by high-resolution magnetic resonance imaging. *Biophys J* 76:103–109, 1999
32. Heyn C, Ronald JA, Mackenzie LT, MacDonald IC, Chambers AF, Rutt BK, Foster PJ: In vivo magnetic resonance imaging of single cells in mouse brain with optical validation. *Magn Reson Med* 55:23–29, 2006
33. Foster-Gareau P, Heyn C, Alejski A, Rutt BK: Imaging single mammalian cells with a 1.5 T clinical MRI scanner. *Magn Reson Med* 49:968–971, 2003
34. Olfert E, Cross BM, McWilliam AA: *Responsibility for the Care and Use of Experimental Animals*. Ottawa, Association of Universities and Colleges of Canada, 1993
35. Fritschy WM, van Suylichem PT, Wolters GH, van Schilfgaarde R: Comparison of top and bottom loading of a dextran gradient for rat pancreatic islet purification. *Diabetes Res* 19:91–95, 1992
36. Frank JA, Miller BR, Arbab AS, Zywicke HA, Jordan EK, Lewis BK, Bryant LH Jr, Bulte JW: Clinically applicable labeling of mammalian and stem cells by combining superparamagnetic iron oxides and transfection agents. *Radiology* 228:480–487, 2003
37. de Groot M, de Haan BJ, Keizer PP, Schuurs TA, van Schilfgaarde R, Leuvenink HG: Rat islet isolation yield and function are donor strain dependent. *Lab Anim* 38:200–206, 2004
38. Yang H, Thomas D, Boffa DJ, Ding R, Li B, Muthukumar T, Sharma VK, Lagman M, Luo GX, Kapur S, Liou HC, Hancock WW, Suthanthiran M: Enforced c-REL deficiency prolongs survival of islet allografts1. *Transplantation* 74:291–298, 2002
39. Evgenov NV, Medarova Z, Dai G, Bonner-Weir S, Moore A: In vivo imaging of islet transplantation. *Nat Med* 12:144–148, 2006
40. Jirak D, Kriz J, Herynek V, Andersson B, Girman P, Burian M, Saudek F, Hajek M: MRI of transplanted pancreatic islets. *Magn Reson Med* 52:1228–1233, 2004
41. Kriz J, Jirak D, Girman P, Berkova Z, Zacharovova K, Honsova E, Lodererova A, Hajek M, Saudek F: Magnetic resonance imaging of pancreatic islets in tolerance and rejection. *Transplantation* 80:1596–1603, 2005